ACS Partner Journal

Journal of the American Society for Mass Spectrometry

pubs.acs.org/jasms

Research Article

Improving Ion Mobility Mass Spectrometry of Proteins through Tristate Gating and Optimization of Multiplexing Parameters

Jamie P. Butalewicz, James D. Sanders, Brian H. Clowers, and Jennifer S. Brodbelt*

Cite This: *J. Am. Soc. Mass Spectrom.* 2023, 34, 101−108

Read Online

ACCESS | Metrics & More | Article Recommendations | Supporting Information

ABSTRACT: Coupling drift tube ion mobility (IM) to Fourier transform mass spectrometry (FT-MS) affords the opportunity for gas-phase separation of ions based on size and conformation with high-resolution mass analysis. However, combining IM and FT-MS is challenging because ions exit the drift tube on a much faster time scale than the rate of mass analysis. Fourier transform (FT) and Hadamard transform multiplexing methods have been implemented to overcome the duty-cycle mismatch, offering new avenues for obtaining high-resolution, high-mass-accuracy analysis of mobility-selected ions. The gating methods used to integrate the drift tube with the FT mass analyzer discriminate against the transmission of large, low-mobility ions owing to the well-known gate depletion effect. Tristate gating strategies have been shown to increase ion transmission for drift tube IM-FT-MS systems through implementation of dual ion gating, controlling the quantity and timing of ions through the drift tube to reduce losses of slow-moving ions. Here we present an optimized set of multiplexing parameters for tristate gating ion mobility of several proteins on an Orbitrap mass spectrometer and further report parameters for increased ion transmission and mobility resolution as well as decreased experimental times from 15 min down to 30 s. On average, peak intensities in the arrival time distributions (ATDs) for ubiquitin increased 2.1× on average, while those of myoglobin increased by 1.5× with a resolving power increase on average of 11%.

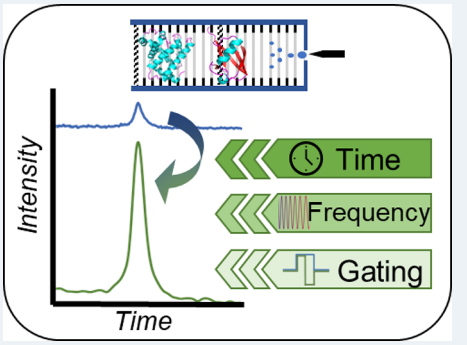

INTRODUCTION

Understanding the structural heterogeneity of proteins and protein complexes in the gas phase remains a challenge even with the advancement of sophisticated tandem mass spectrometry,[1−4] ion mobility methods,[5−11] and new computational programs such as Alpha-Fold.[12,13] Changes imparted through interaction of proteins with ligands or other proteins, addition of post-translational modifications, or adoption of different conformations increases the difficulty of discerning structures.[14−17] Drift tube ion mobility has gained popularity as a way to provide gas-phase separation of heterogeneous ion populations based on their size and shape while allowing the determination of ion-neutral collision cross section (CCS).[18,19]

Drift tube ion mobility (DTIM) separates ions within a uniform electric field, transmitting ions through a designated drift region where the ion velocities are related to their inherent mobility.[18,20,21] The forward motion of the ions is resisted by friction generated through interaction with an inert buffer gas, allowing first-principles calculation of CCS.[17,18] Typically, DTIM systems are interfaced with time-of-flight (TOF) mass spectrometers owing to their fast scan rates and ability to sample the ions in real time as they exit the drift tube.[20] Other IM platforms such as traveling wave (TWIMS),[22,23] trapped (TIMS),[24] and field-asymmetric waveform (FAIMS)[25] are routinely adapted for TOF instruments and have been incorporated into a number of commercial platforms. Although these systems are becoming increasingly common, often their resolution and tandem MS (MS/MS) capabilities limit their utility in the analysis of more complex analytes such as intact proteins. Orbitrap mass spectrometers[26] provide enhanced mass resolution and MS/MS functionality but operate at significantly slower scan speeds (hundreds of milliseconds) than ion mobility separations (tens of milliseconds), posing a challenge for integration of drift tubes with high-performance mass analysis. Because of this duty-cycle mismatch, DTIM-Orbitrap instruments typically employ two electrostatic ion gates at the entrance and exit of the drift tube, which can be operated in such a way as to allow only ions with a specified drift time to be transmitted to the mass spectrometer.[5,7,9,11,17,27−29] Fourier transform (FT) multiplexing can be used to improve the duty cycle of standard dual-gate drift tube IM-MS systems and generate full arrival time distributions (ATDs) with improved sensitivity and shorter acquisition times.[10,27,30−32] Through systematic modulation of the front and back gates of the drift tube using a swept frequency square waveform, the ion drift times are

Received: September 23, 2022
Revised: November 21, 2022
Accepted: November 23, 2022
Published: December 5, 2022

https://doi.org/10.1021/jasms.2c00274
J. Am. Soc. Mass Spectrom. 2023, 34, 101−108

encoded as oscillations within ion current on the mass spectrometer.[29,32] Extracted ion chromatograms (XICs) can be used to selectively map the ion current for each m/z of interest prior to FT to generate m/z-specific ATDs.

Although FT-multiplexing has become a widely used method to overcome the aforementioned duty-cycle mismatch, two problems remain unresolved in the context of analysis of proteins: (1) mobility discrimination resulting from gate depletion and (2) the need for significant signal averaging results in low throughput. For DTIM systems that operate using electrostatic ion gates, the gate depletion effect suppresses low-mobility ions as they traverse the gating region. This effect causes rapid decay rates of the ion current oscillations within the XICs and therefore results in significant losses in sensitivity and increased background noise within the ATDs.[30,33,34] Various ion gate designs have been devised to modulate both front and back gates of a drift tube to enhance sensitivity of lower mobility ions, i.e., ions with larger collision cross sections. Bradbury-Nielsen,[35] Tyndall-Powell,[36] trigrid,[34] and other ion shutter architectures[37,38] have previously demonstrated large "cutting zones" within gating that result in the loss of slow-moving ions. Further modifications to the drift tube itself to perform overtone mobility experiments and reduce ion losses have also been undertaken.[39,40] As shown schematically in Figure 1, the cutting zone is a mobility-dependent region where lower mobility ions cannot effectively traverse the physical plane of the ion gate used to modulate the ion beam, resulting in discrimination in the observed mobility spectra. When a shutter is opened, ions traverse through the region until the shutter is closed, with the faster moving ions making it through the gate while the slower moving ions are cut off. The size of this "cutting zone" varies by gate design but consistently has remained a problem for ion transmission for lower mobility ions.[30,33,34] Lengthy acquisition times and the need for extensive signal averaging to compensate for these difficulties further limit experimental throughput. These factors contribute to a significant disadvantage for analysis of low-mobility protein ions that often exist in low abundances owing to dispersion among many charge states and conformations.

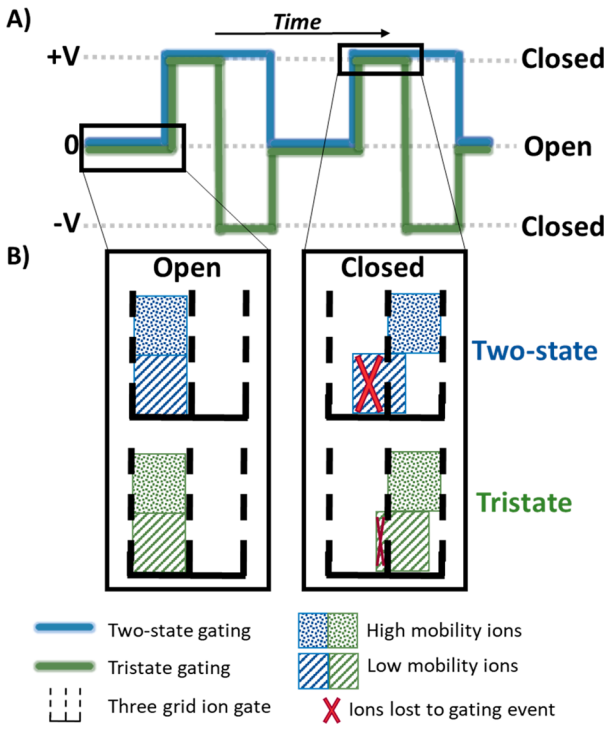

Figure 1. Gating schemes imparted on the two electrostatic trigrid gates of the DTIM-FT-MS system. (A) Two-state gating (blue) and tristate gating (green) waveforms imparted on the gates denoting the corresponding "open" and "closed" states of the grid and (B) ion populations representing low- and high-mobility ions traversing the trigrid gate while in open and closed states. Tristate gating reduces the low-mobility ion population that is lost in the closed gating states.

A method termed tristate gating was recently introduced[34] to minimize the cutting region and minimize the bias against slow-moving ions caused by the gate depletion effect.[30,34] As previously described, a three-grid shutter is used to generate two distinct cutting zones that can be modulated by applying either a positive or negative potential on the second grid (Figure 1).[30,34] By initially applying a negative potential, the elimination zone is created between the second and third grids, allowing ions to traverse from the ionization or desolvation region through to the second grid. The supplemental voltage on the second grid is removed to restore the voltage gradient used to push ions through the region. As the ions move through the gate region, a positive potential is then applied to the second grid, generating an elimination zone between the first and second grids. Ions that have traversed past the second grid will be pushed into the drift region, while those in the elimination zone will be lost. Because the packet of ions that is injected into the drift region start at the second grid and are further truncated at the same location through a shifting of the elimination zone, the bias against the slower moving ions can be reduced, and the ions will traverse a distance appropriate to their inherent mobilities. Tristate gating has been shown to increase the ion abundance as well as the resolving power observed within the arrival time distribution.[30,33,34,38,41,42] Direct comparison of the tristate gating method to two-state gating methods was performed using a series of tetraalkylammonium salts and further demonstrated for higher resolution separation of isomeric peptides.[30,33,42] Other studies have validated this approach as a reliable method for reducing the effects of gating bias,[34,38,41] but to date, these methods have not been implemented for ion mobility applications of large molecules, such as proteins.

Further optimization of the multiplexing technique offers the potential for more effective ion mobility separation of protein ions with much greater throughput.[10,17] The end frequency of an FT-IM sweep directly influences the density of data points in the generated ATD and therefore has a substantial impact on the maximum resolving power that can be attained. When very high ending frequencies of the sweep are used in comparison to the starting frequency, the spacing between data points in the ATD becomes inversely proportional to the end frequency itself. In general, a lower end frequency will lead to lower resolving powers but must be balanced against overall sweep rates as well as the ions drift time. While the greatest theoretical resolving powers should be generated with high end frequencies and slow sweep rates, new Orbitrap FT-MS systems offering faster scan times through multiplexed analysis allow the potential to maintain moderate end frequencies and significantly increased sweep rates while preserving the high resolving powers necessary to distinguish large biological molecules. We report here the use of tristate gating with optimized multiplexing parameters to probe the ability to

https://doi.org/10.1021/jasms.2c00274
J. Am. Soc. Mass Spectrom. 2023, 34, 101−108

analyze proteins with drift tube ion mobility coupled to a high-performance Orbitrap mass spectrometer.

METHODS

Chemicals and Materials. Ubiquitin from bovine erythrocytes, myoglobin from equine skeletal muscle, cytochrome C from equine heart, and tetraalkylammonium bromide salts (TAA) were purchased from Sigma-Aldrich (St Louis, MO), and angiotensin I was purchased from Genscript (Piscataway, NJ). All samples were used without further modification or purification. Each protein or peptide was dissolved in a 50/50 mixture of methanol/water with 0.1% formic acid to a final concentration of 10 μM. TAA salts with alkyl chains ranging from 5 to 12 carbons were individually dissolved in methanol prior to combination of the salts in 50/50 methanol/water to a final concentration of 10 μM.

Instrumentation. An atmospheric pressure drift tube was mounted to the front end of a Q-Exactive HF-X BioPharma Orbitrap mass spectrometer (Thermo Fisher Scientific, San Jose, CA), (Figure 2). The drift tube was constructed as described in detail previously.[8,43] A nanoelectrospray source using gold palladium coated emitters pulled in-house and with a spray voltage of 1.0−1.5 kV floated above the drift voltage was used to generate ions. The drift tube consists of a ∼10 cm desolvation region followed by a ∼10 cm drift region. A voltage of 10 kV is applied to the ring electrodes connected through a chain of resistors that span the length of the drift tube, used to generate the uniform electric field throughout. Three-grid ion gates are located at the front and back ends of the drift region and operated independently using FET pulsers designed and built by GAA Custom Engineering.[44] Three-grid gates have been reported previously and have not been shown to contribute to ion losses compared to two-grid systems.[42] Dependent on the gating mechanism, either one or two FET pulsers were used per gate and controlled using a custom program written in LabView and a National Instruments PXI 6289 module (National Instruments, Austin, TX). The LabView program generates and outputs an increasing frequency square waveform from user input values of start and end frequency as well as sweep time with a selection of the desired gating method. The waveform triggers high/low outputs from the pulsers, which are configured individually to output optimized gating potentials, described further in the Results section. For tristate gating, each gate is modulated with two FET pulsers wired in tandem to supply both positive and negative potentials, while two-state gating methods require only one pulser per gate.

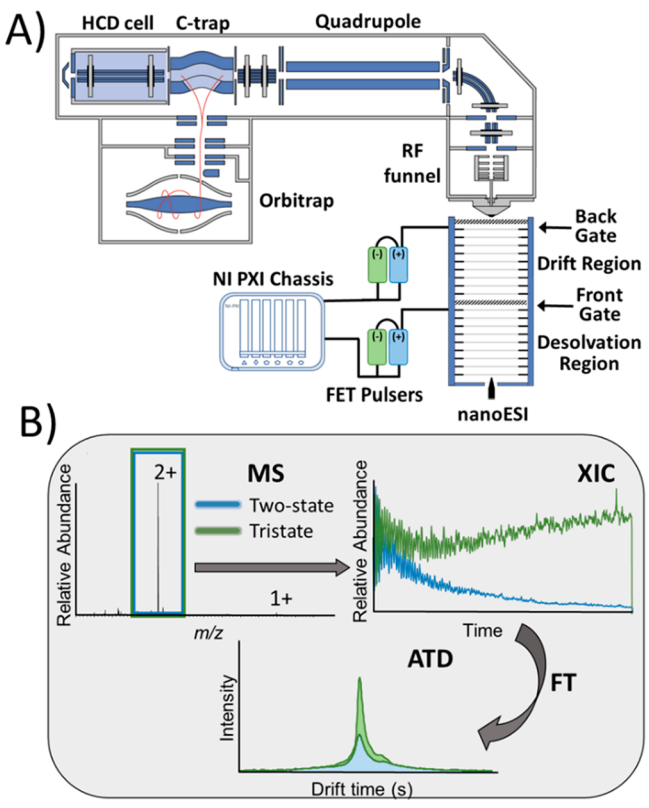

Figure 2. (A) Instrument schematic. Ions are generated through a nanoESI emitter at the front end of the atmospheric pressure drift tube. The two gates of the drift tube are controlled using waveforms generated through National Instruments software and FET Pulsers. The drift tube is interfaced to the front end of a Q-Exactive HF-X Orbitrap mass spectrometer. (B) Typical experimental workflow entails acquisition of mass spectra, generation of extracted ion chromatograms (XICs) for each ion of interest using two-state and tristate gating methods, and Fourier transformation of the XICs to generate arrival time distributions (ATDs).

In a typical experiment, the gating frequency is swept from 5 to 5000 Hz in a period ranging from 1 to 15 min.[17,32] Simultaneously, mass spectra are acquired in the Orbitrap mass spectrometer where the ion injection time was fixed to retain consistent scan times across experiments. Extracted ion chromatograms (XICs) are generated for each ion of interest, showing a distinct ion current that oscillates with a frequency unique to the ion's drift time. XICs are extracted, triplicates are averaged, and further processing is performed by Fourier transformation using standard magnitude mode or absorption mode with a custom written Matlab code.[8] Thereafter, m/z-dependent arrival time distributions are produced, and further statistical analysis to extract drift times, signal-to-noise, and resolving power is performed using a supplemental custom Matlab program.

RESULTS AND DISCUSSION

Optimization of Multiplexing and Standard Gating Parameters. Prior to implementing the tristate gating strategy, the multiplexing and gating parameters for the DTIM-FT-MS experiments were optimized. Benchmarking and optimization experiments were undertaken with ubiquitin (8.6 kDa protein) in 6+ to 13+ charge states. ATDs are then processed to calculate S/N, resolving power (RP), and other figures of merit.

Optimization of Sweep Rate. For FT-MS systems, mass resolution depends on scan speed. To acquire a high-resolution mass spectrum in an Orbitrap analyzer, transients extending hundreds of milliseconds are acquired. Although FT-multiplexing overcomes the mismatch in duty cycles between ion mobility sweep time and mass analysis, the slower speeds of the mass scan require the use of larger frequency ranges and sweep times in order to adequately sample the ion current modulation in the time domain. To optimize MS conditions for the highest IM resolving power and signal-to-noise (S/N), standard FT-IMS sweeps were collected using various mass resolutions with corresponding transient times of 512, 256, 128, 64, and 32 ms for ubiquitin. Ion injection times were kept shorter than the transient time for each particular mass resolution to prevent further increases of the duty cycle. The

https://doi.org/10.1021/jasms.2c00274
J. Am. Soc. Mass Spectrom. 2023, 34, 101−108

S/N and IM resolving power were calculated based on the 5+ through 11+ charge states of ubiquitin in Figure S1 and Table S1. While little difference in S/N and resolving power was noted for previous analysis of the TAA ions across the various MS resolutions, several charge states of ubiquitin displayed a significant increase in S/N at higher mass resolutions (i.e., acquisition of longer transients). While low mass resolutions with fast transient scan times (i.e., 32 ms) are most beneficial in tandem with drift tube analysis for small ions, for many charge states of larger protein ions, the greatest increases in ion mobility figures of merit are achieved through moderate mass resolution with longer transient times (i.e., 256 ms).

The sweep rate determines how many frequencies are encoded within each data point of the resulting XIC; a faster sweep rate will encode more frequencies into each data point and lower the resulting IM resolving power.[45] The end frequency of a sweep determines the number of data points sampled for a peak of interest within the ATD as well as the subsequent resolving power, which can be further augmented through the use of apodization and zero padding of the XIC prior to Fourier transformation.[8] The fastest sweep rate that can be achieved is governed by the Nyquist theorem, which states that the encoding frequency of the drift time being measured (f_{en}) is proportional to the sweep rate (f_{en} = sweep rate/drift time).[8] The sweep rate then must be kept at or below half the scan rate of the mass spectrometer, which for the Orbitrap mass spectrometer used in the present study that employs multiplexing is equivalent to the transient time. In short, the longest drift time within the experiment will have an encoding frequency, which will govern the sweep rate depending on the mass resolution being used. In typical experiments, the Nyquist limit is not approached owing to long transient times, complex samples, or poor ion transmission that impedes the practical use of the faster sweep rates.

To assess the experimental throughput (i.e., duration of data acquisition and sweep times needed) and the ability to approach the Nyquist limit, standard FT-IM sweeps of 5 to 5000 Hz in 15 to 0.5 min were conducted to represent sweep rates of 5.55 to 166.50 Hz/s. In each case, S/N and resolving power were determined from the ATDs of the 10+ to 12+ charge states of ubiquitin. Figure 3 shows the resulting S/N and resolving powers as a function of sweep rate with error bars generated through triplicate experiments, collected on the same day. The greatest variation in the standard deviations of S/N was observed for the longest sweep times of 10 and 15 min, while little variation in resolving power was seen. Owing to the large abundance of protein ions, minor fluctuations in temperature and pressure should not substantially change the fwhm of the peak or drift time within the ATD and therefore not affect RP; however, background ions of low abundance are more likely to vary and contribute to variations in S/N. The RP and S/N observed across protein charge states varied little with decreased sweep times from 15 min down to 30 s, demonstrating that respectable results in significantly shorter experimental times can be achieved. The impact of using extremely fast sweep rates on the analysis of larger proteins was not investigated further. A baseline sweep rate of 16.6 Hz/s was chosen for additional optimization and assessment of gating performance because it provided the most consistent balance between attaining high-quality mass spectra and reasonable experimental throughput. It is worth noting, however, that there is a maximum sweep rate that can be applied during the FT-IM experiment, above which aliasing

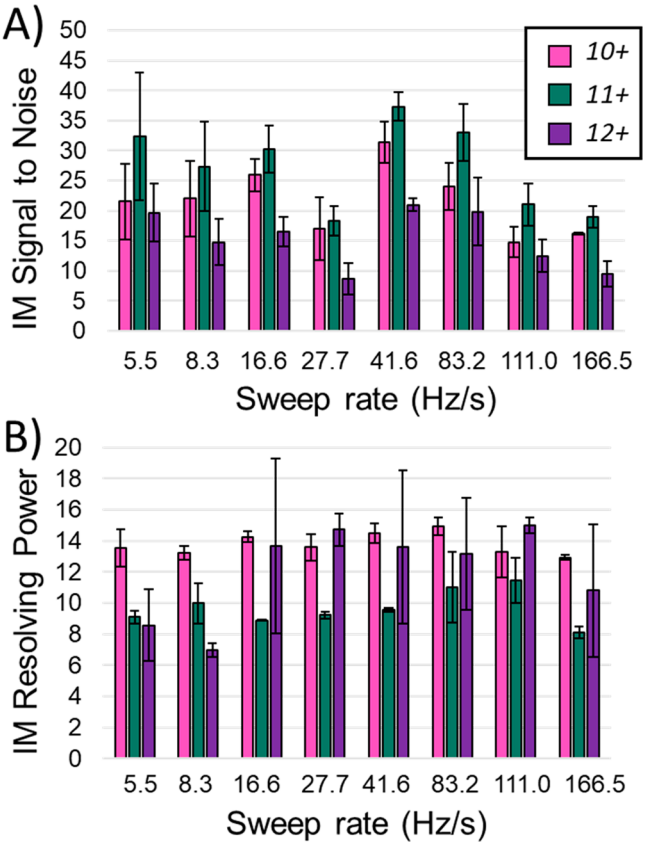

Figure 3. (A) S/N and (B) resolving power as a function of sweep rate for three charge states of ubiquitin (10+ in pink, 11+ in green, 12+ in purple) based on triplicate measurements collected on the same day.

may occur.[46] Overall, increasing the sweep rate to 16.6 Hz/s resulted in no significant decrease in IM S/N or resolving power, demonstrating the ability to approach the Nyquist limit while maintaining data quality.

The impact of the terminal sweep frequency on the S/N and resolving power was also examined. Using 5 and 1 min sweep times, the terminal frequency was varied between 10 000 and 1000 Hz. Figure 4 shows the calculated S/N and RP overlaid on the ATD acquired for the 10+ charge state of ubiquitin. Although the S/N is greatest using the 1000 Hz terminal sweep frequency, the RP is also significantly decreased. For a 5 min sweep, a terminal sweep frequency of 3000 or 5000 Hz was optimal, whereas reducing the sweep time to 1 min afforded better S/N and RP for a terminal sweep frequency of 3000 Hz. This trend is consistent with the space charge broadening effect; as the terminal frequency of the sweep is decreased and therefore the resulting sweep rate is decreased, we observe band broadening in the ATD that is likely due to the increase in the ion population within the drift region.[47] For the remainder of experiments, a 5 min sweep with a terminal frequency of 5000 Hz resulting in a 16.65 Hz/s sweep was used unless otherwise noted.

Optimization of Gate Voltages. In addition to influencing the transmission of all ions though the drift region and into the mass spectrometer, the voltages applied to the gates may also bias the transmission of the slow-moving ions. The impact of the front and back gate voltages on transmission of ions was evaluated for angiotensin, ubiquitin, and myoglobin. For this evaluation, the voltage applied to one gate was serially

https://doi.org/10.1021/jasms.2c00274
J. Am. Soc. Mass Spectrom. 2023, 34, 101−108

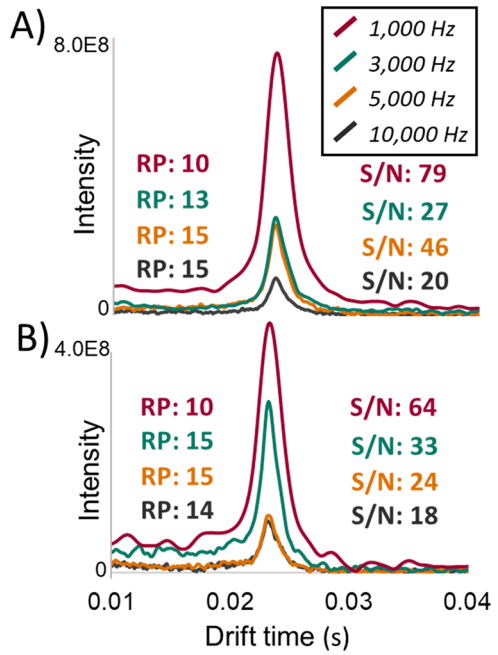

Figure 4. Impact of terminal sweep frequency on resolving power and S/N of the ATDs of ubiquitin (10+) acquired for (A) 5 min sweep or (B) 1 min sweep with a starting frequency of 5 Hz.

increased from 10 to 100 V, while the other gate was electrically connected to the drift tube voltage gradient to disconnect its gating function. Ion current in the Orbitrap analyzer was used to estimate transmission as a function of the front and back gate voltages, as illustrated in Figure S2. The transmission data collected at each gate voltage were fit with a standard polynomial curve, and the lowest gate voltage that prevented transmission of ions was determined. These voltages were 65 and 80 V for the front and back gates, respectively, and these gating potentials were used for the remainder of the experiments.

Gating: Tristate vs Two-State. With multiplexing and FTIMS parameters fully optimized for maximum IM resolving power and S/N, the drift tube gating methods were tested and compared for overall performance of protein analysis. The same gating voltages and sweep parameters were applied for both two-state and tristate gating methods, and all spectra were collected the same day with the same nanoelectrospray emitter. The gating frequency was swept from 5 to 5000 Hz, and mass spectra were collected in the Orbitrap analyzer at 120 00 resolution. The data processing workflow is shown in Figure 2B. The mass spectra collected were compared for each gating method, and identical charge state distributions were observed. Moreover, given that the experiments were conducted at low electric field strengths and atmospheric pressure, there is no expectation that field contributions to the ion velocity contributed to any differences between the ion gating methods. XICs were generated in triplicate and averaged for each charge state of interest from the mass spectra and then subjected to Fourier transformation to produce an ATD. The ATD for each gating method was then statistically processed to determine IM resolving power and S/N and overlaid to allow direct comparison of peak shapes and relative intensities.

The ATDs generated for several charge states of ubiquitin are shown in Figure 5. The relative peak intensity increases approximately 2-fold for the tristate gating method relative to

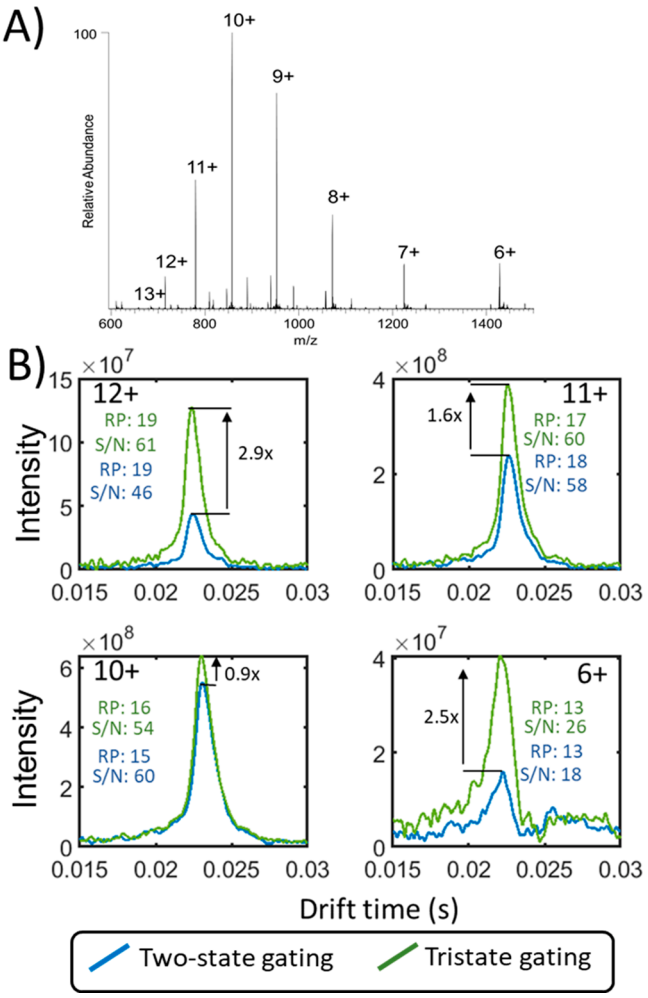

Figure 5. (A) Mass spectrum of ubiquitin and (B) corresponding ATDs collected with two-state gating (blue) and tristate gating (green) for various charge states. The calculated resolving power and resulting S/ N for each gating method as well as the increase in relative intensity are listed for each ATD.

the two-state method, but there is little change in the resolving power between the two methods. The increase in peak intensity appears to be more significant for the charge states of lower abundance. For example, the 6+ charge state produces a two-state gating ATD with a S/N value of 18 and resolving power of 13 increasing to S/N 26 and resolving power of 13. The S/N of the 12+ charge state increases from 46 to 68 for the tristate gating method with a 2.9× increase in peak intensity. The average peak intensity increase across all charge states with one conformer present was 109%. The ATDs for all charge states of ubiquitin are compared in Figure S3, and all calculated figures of merit are summarized in Table S2. Statistical analysis was performed utilizing *t* tests to generate *p*-values as well as standard deviations based on replicate gating experiments, summarized in Table S4. While a majority of charge states displayed statistically significant increases in the S/N with tristate gating (four out of five charge states), the increases in resolving power were not significant (only one out of five charge states showed an increase in resolving power). The similarities in resolving power between the two gating methods indicate that the full width half max values of the peaks and the drift times remained consistent without distortion in peak shape or drift times.

https://doi.org/10.1021/jasms.2c00274
J. Am. Soc. Mass Spectrom. 2023, 34, 101−108

Comparisons of the two gating methods were also undertaken for myoglobin (17 kDa, 9+ to 22+ charge states). Figure S4 shows the representative MS1 spectrum and corresponding ATD for selected charge states. For the higher charge states (18+ to 22+) that exhibit a single mobility peak, significant increases in both peak intensity (averaging 49%) and resolving power (averaging 11%) are observed. The ATDs for all charge states of myoglobin are compared in Figure S5, and all calculated figures of merit are summarized in Table S3. The statistical analysis is summarized in Table S4. The greatest improvements in resolution for the tristate gating method occur for the 15+ and 16+ charge states, each appearing to have two mobility features that may represent different conformers. Conformation distributions of the charge states matched well with a previous report.[48] To calculate the resolution between the two putative conformers of the 16+ charge state, the raw data were baseline-corrected in MATLAB and fit with the sum of two Gaussians to extract fwhm values. To minimize any error between fits, constraining factors to the Gaussian fits were held constant between different data sets. Figure 6 shows the Gaussian fits overlaid on the baseline-

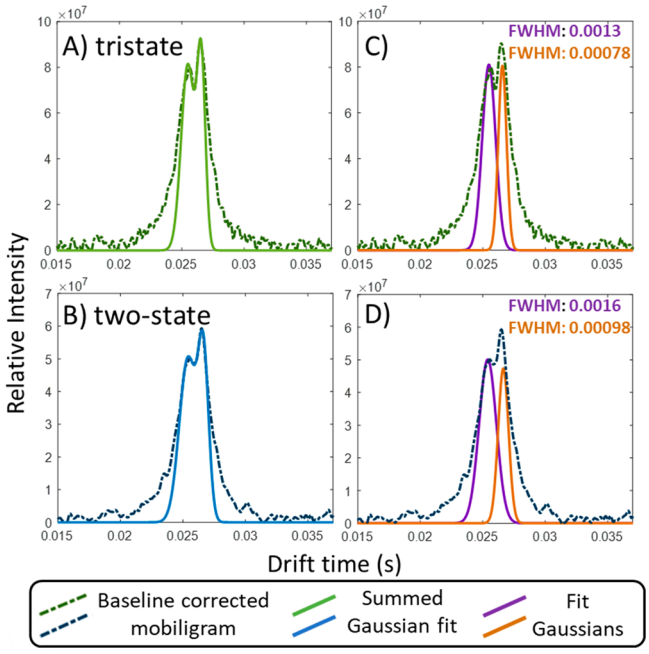

Figure 6. ATDs generated for the 16+ charge state of myoglobin were baseline-corrected and fit with the sum of two Gaussians for (A) tristate gating and (B) two-state gating. The two individual Gaussians were overlaid with the summed fit ((C) tristate, (D) two-state), and the resulting fwhm of each peak was extracted.

corrected ATDs. Two-state gating yielded a resolution of 0.7, whereas tristate gating afforded an approximate resolution of 0.9 for the 16+ charge state, a ~33% increase in resolution. The increase in resolution was ~25% for the 15+ charge state of myoglobin using the tristate gating method (Figure S7). Due to the ability of tristate gating to reduce bias against larger, slow-moving ions, it is expected that greater ion transmission of the multiple myoglobin conformations contributed to this higher resolution of both 16+ and 15+ charge states.

Cytochrome c (12 kDa, 6+ to 17+ charge states) proved to be an outlier. Figure S6 shows the MS1 spectrum as well as the ATDs for the 13+ and 15+ charge states. The ATDs for all charge states of cytochrome c are further compared in Figure S6c. In contrast to the other proteins analyzed, tristate gating did not produce improvements in S/N or resolving power. Signal abundances between both tristate and two-state gating methods were comparable across most charge states, with several showing higher signal from the standard two-state gating. We attribute this result to the greater conformational heterogeneity of cytochrome c, as reported in several prior ion mobility studies.[48−50] The improved tristate gating method does not offer sufficiently high resolving power to overcome this heterogeneity.

CONCLUSIONS

Drift tube IM-FT-MS methods were optimized for the analysis of intact proteins through detailed analysis of sweep parameters with respect to MS scan rates. The resolving power and S/N observed across protein charge states varied little with sweep times decreased from 15 min down to 30 s. These results suggest that multiplexed FT-IMS experiments could approach the rapid time scale of DTIM-TOF or TIMS-TOF instruments, significantly increasing the throughput of typical DTIM-FTMS experiments. Optimization of sweep end frequency, MS resolution, and sweep rate maximized the signal abundance and yielded minimal improvements in S/N and resolving power for the analysis of proteins. Tristate gating was employed to reduce the gating bias against slow-moving ions, which impacts the analysis of proteins. For ubiquitin and myoglobin, overall signal intensity increased 2 to 3× for most charge states, and modest improvements in resolving power and S/N were noted in some cases. In the case of partially resolved peaks, tristate gating improved the resolution between peaks by up to 36%. While the size of the cutting regions has been reduced with tristate gating, apparent through increased signal intensity as well as S/N, RP, or resolution improvements, further optimization of these methods to eliminate the cutting region should allow reduced experimental times and enhanced characterization of native proteins and their complex conformations. Overall, through the use of tristate gating and the extensive optimization of multiplexing parameters, the throughput and analysis of proteins were enhanced for atmospheric pressure drift tube IM-FT-MS experiments.

ASSOCIATED CONTENT

Supporting Information

The Supporting Information is available free of charge at https://pubs.acs.org/doi/10.1021/jasms.2c00274.

Figures of merit for MS optimization, gate voltage-dependent ion depletion plots for proteins and a peptide, arrival time distributions generated for ubiquitin/myoglobin/cytochrome C in both two-state and tristate gating methods, and all associated figures of merit corresponding to the gating experiments (PDF)

AUTHOR INFORMATION

Corresponding Author

Jennifer S. Brodbelt − *Department of Chemistry, The University of Texas at Austin, Austin, Texas 78712, United States;* orcid.org/0000-0003-3207-0217; Email: jbrodbelt@cm.utexas.edu

Authors

Jamie P. Butalewicz − *Department of Chemistry, The University of Texas at Austin, Austin, Texas 78712, United States*

James D. Sanders − *Department of Chemistry, The University of Texas at Austin, Austin, Texas 78712, United States*

Brian H. Clowers − *Department of Chemistry, Washington State University, Pullman, Washington 99164, United States;* orcid.org/0000-0002-5809-9379

Complete contact information is available at: https://pubs.acs.org/10.1021/jasms.2c00274

Notes

The authors declare no competing financial interest.

■ ACKNOWLEDGMENTS

We acknowledge the following funding sources: NSF (Grant CHE-2203602) and the Welch Foundation (Grant F-1155).

■ REFERENCES

(1) O'Brien, J. P.; Li, W.; Zhang, Y.; Brodbelt, J. S. Characterization of Native Protein Complexes Using Ultraviolet Photodissociation Mass Spectrometry. *J. Am. Chem. Soc.* **2014**, *136* (37), 12920−12928.

(2) Zhou, M.; Lantz, C.; Brown, K. A.; Ge, Y.; Paša-Tolić, L.; Loo, J. A.; Lermyte, F. Higher-Order Structural Characterisation of Native Proteins and Complexes by Top-down Mass Spectrometry. *Chem. Sci.* **2020**, *11* (48), 12918−12936.

(3) Tucholski, T.; Ge, Y. Fourier-Transform Ion Cyclotron Resonance Mass Spectrometry for Characterizing Proteoforms. *Mass Spectrom. Rev.* **2022**, *41* (2), 158−177.

(4) Tamara, S.; den Boer, M. A.; Heck, A. J. R. High-Resolution Native Mass Spectrometry. *Chem. Rev.* **2022**, *122* (8), 7269−7326.

(5) Sanders, J. D.; Shields, S. W.; Escobar, E. E.; Lanzillotti, M. B.; Butalewicz, J. P.; James, V. K.; Blevins, M. S.; Sipe, S. N.; Brodbelt, J. S. Enhanced Ion Mobility Separation and Characterization of Isomeric Phosphatidylcholines Using Absorption Mode Fourier Transform Multiplexing and Ultraviolet Photodissociation Mass Spectrometry. *Anal. Chem.* **2022**, *94* (10), 4252−4259.

(6) Zheng, X.; Kurulugama, R. T.; Laganowsky, A.; Russell, D. H. Collision-Induced Unfolding Studies of Proteins and Protein Complexes Using Drift Tube Ion Mobility-Mass Spectrometer. *Anal. Chem.* **2020**, *92* (10), 7218−7225.

(7) McCabe, J. W.; Mallis, C. S.; Kocurek, K. I.; Poltash, M. L.; Shirzadeh, M.; Hebert, M. J.; Fan, L.; Walker, T. E.; Zheng, X.; Jiang, T.; Dong, S.; Lin, C.-W.; Laganowsky, A.; Russell, D. H. First-Principles Collision Cross Section Measurements of Large Proteins and Protein Complexes. *Anal. Chem.* **2020**, *92* (16), 11155−11163.

(8) Sanders, J. D.; Butalewicz, J. P.; Clowers, B. H.; Brodbelt, J. S. Absorption Mode Fourier Transform Ion Mobility Mass Spectrometry Multiplexing Combined with Half-Window Apodization Windows Improves Resolution and Shortens Acquisition Times. *Anal. Chem.* **2021**, *93* (27), 9513−9520.

(9) Sipe, S. N.; Sanders, J. D.; Reinecke, T.; Clowers, B. H.; Brodbelt, J. S. Separation and Collision Cross Section Measurements of Protein Complexes Afforded by a Modular Drift Tube Coupled to an Orbitrap Mass Spectrometer. *Anal. Chem.* **2022**, *94* (26), 9434−9441.

(10) McKenna, K. R.; Clowers, B. H.; Krishnamurthy, R.; Liotta, C. L.; Fernández, F. M. Separations of Carbohydrates with Noncovalent Shift Reagents by Frequency-Modulated Ion Mobility-Orbitrap Mass Spectrometry. *J. Am. Soc. Mass Spectrom.* **2021**, *32*, 2472.

(11) Ibrahim, Y. M.; Garimella, S. V. B.; Prost, S. A.; Wojcik, R.; Norheim, R. V.; Baker, E. S.; Rusyn, I.; Smith, R. D. Development of an Ion Mobility Spectrometry-Orbitrap Mass Spectrometer Platform. *Anal. Chem.* **2016**, *88* (24), 12152−12160.

(12) Jumper, J.; Evans, R.; Pritzel, A.; Green, T.; Figurnov, M.; Ronneberger, O.; Tunyasuvunakool, K.; Bates, R.; Žídek, A.; Potapenko, A.; Bridgland, A.; Meyer, C.; Kohl, S. A. A.; Ballard, A. J.; Cowie, A.; Romera-Paredes, B.; Nikolov, S.; Jain, R.; Adler, J.; Back, T.; Petersen, S.; Reiman, D.; Clancy, E.; Zielinski, M.; Steinegger, M.; Pacholska, M.; Berghammer, T.; Bodenstein, S.; Silver, D.; Vinyals, O.; Senior, A. W.; Kavukcuoglu, K.; Kohli, P.; Hassabis, D. Highly Accurate Protein Structure Prediction with AlphaFold. *Nature* **2021**, *596* (7873), 583−589.

(13) Senior, A. W.; Evans, R.; Jumper, J.; Kirkpatrick, J.; Sifre, L.; Green, T.; Qin, C.; Žídek, A.; Nelson, A. W. R.; Bridgland, A.; Penedones, H.; Petersen, S.; Simonyan, K.; Crossan, S.; Kohli, P.; Jones, D. T.; Silver, D.; Kavukcuoglu, K.; Hassabis, D. Improved Protein Structure Prediction Using Potentials from Deep Learning. *Nature* **2020**, *577* (7792), 706−710.

(14) Clemmer, D. E.; Russell, D. H.; Williams, E. R. Characterizing the *Conformationome*: Toward a Structural Understanding of the Proteome. *Acc. Chem. Res.* **2017**, *50* (3), 556−560.

(15) Aebersold, R.; Agar, J. N.; Amster, I. J.; Baker, M. S.; Bertozzi, C. R.; Boja, E. S.; Costello, C. E.; Cravatt, B. F.; Fenselau, C.; Garcia, B. A.; Ge, Y.; Gunawardena, J.; Hendrickson, R. C.; Hergenrother, P. J.; Huber, C. G.; Ivanov, A. R.; Jensen, O. N.; Jewett, M. C.; Kelleher, N. L.; Kiessling, L. L.; Krogan, N. J.; Larsen, M. R.; Loo, J. A.; Loo, R. R. O.; Lundberg, E.; MacCoss, M. J.; Mallick, P.; Mootha, V. K.; Mrksich, M.; Muir, T. W.; Patrie, S. M.; Pesavento, J. J.; Pitteri, S. J.; Rodriguez, H.; Saghatelian, A.; Sandoval, W.; Schlüter, H.; Sechi, S.; Slavoff, S. A.; Smith, L. M.; Snyder, M. P.; Thomas, P. M.; Uhlén, M.; Van Eyk, J. E.; Vidal, M.; Walt, D. R.; White, F. M.; Williams, E. R.; Wohlschlager, T.; Wysocki, V. H.; Yates, N. A.; Young, N. L.; Zhang, B. How Many Human Proteoforms Are There? *Nat. Chem. Biol.* **2018**, *14* (3), 206−214.

(16) McLean, J. A.; Ruotolo, B. T.; Gillig, K. J.; Russell, D. H. Ion Mobility−Mass Spectrometry: A New Paradigm for Proteomics. *Int. J. Mass Spectrom.* **2005**, *240* (3), 301−315.

(17) Poltash, M. L.; McCabe, J. W.; Shirzadeh, M.; Laganowsky, A.; Clowers, B. H.; Russell, D. H. Fourier Transform-Ion Mobility-Orbitrap Mass Spectrometer: A Next-Generation Instrument for Native Mass Spectrometry. *Anal. Chem.* **2018**, *90* (17), 10472−10478.

(18) Dodds, J. N.; Baker, E. S. Ion Mobility Spectrometry: Fundamental Concepts, Instrumentation, Applications, and the Road Ahead. *J. Am. Soc. Mass Spectrom.* **2019**, *30* (11), 2185−2195.

(19) Stow, S. M.; Causon, T. J.; Zheng, X.; Kurulugama, R. T.; Mairinger, T.; May, J. C.; Rennie, E. E.; Baker, E. S.; Smith, R. D.; McLean, J. A.; Hann, S.; Fjeldsted, J. C. An Interlaboratory Evaluation of Drift Tube Ion Mobility−Mass Spectrometry Collision Cross Section Measurements. *Anal. Chem.* **2017**, *89* (17), 9048−9055.

(20) Kanu, A. B.; Dwivedi, P.; Tam, M.; Matz, L.; Hill, H. H., Jr. Ion Mobility−Mass Spectrometry. *J. Mass Spectrom.* **2008**, *43* (1), 1−22.

(21) Gabelica, V.; Shvartsburg, A. A.; Afonso, C.; Barran, P.; Benesch, J. L. P.; Bleiholder, C.; Bowers, M. T.; Bilbao, A.; Bush, M. F.; Campbell, J. L.; Campuzano, I. D. G.; Causon, T.; Clowers, B. H.; Creaser, C. S.; De Pauw, E.; Far, J.; Fernandez-Lima, F.; Fjeldsted, J. C.; Giles, K.; Groessl, M.; Hogan, C. J., Jr; Hann, S.; Kim, H. I.; Kurulugama, R. T.; May, J. C.; McLean, J. A.; Pagel, K.; Richardson, K.; Ridgeway, M. E.; Rosu, F.; Sobott, F.; Thalassinos, K.; Valentine, S. J.; Wyttenbach, T. Recommendations for Reporting Ion Mobility Mass Spectrometry Measurements. *Mass Spectrom. Rev.* **2019**, *38* (3), 291−320.

(22) Shvartsburg, A. A.; Smith, R. D. Fundamentals of Traveling Wave Ion Mobility Spectrometry. *Anal. Chem.* **2008**, *80* (24), 9689−9699.

(23) Garimella, S. V. B.; Ibrahim, Y. M.; Webb, I. K.; Tolmachev, A. V.; Zhang, X.; Prost, S. A.; Anderson, G. A.; Smith, R. D. Simulation of Electric Potentials and Ion Motion in Planar Electrode Structures for Lossless Ion Manipulations (SLIM). *J. Am. Soc. Mass Spectrom.* **2014**, *25* (11), 1890−1896.

(24) Michelmann, K.; Silveira, J. A.; Ridgeway, M. E.; Park, M. A. Fundamentals of Trapped Ion Mobility Spectrometry. *J. Am. Soc. Mass Spectrom.* **2015**, *26* (1), 14−24.

(25) Barnett, D. A.; Ells, B.; Guevremont, R.; Purves, R. W.; Viehland, L. A. Evaluation of Carrier Gases for Use in High-Field Asymmetric Waveform Ion Mobility Spectrometry. *J. Am. Soc. Mass Spectrom.* **2000**, *11* (12), 1125−1133.
(26) Eliuk, S.; Makarov, A. Evolution of Orbitrap Mass Spectrometry Instrumentation. *Annu. Rev. Anal. Chem.* **2015**, *8* (1), 61−80.
(27) Reinecke, T.; Davis, A. L.; Clowers, B. H. Determination of Gas-Phase Ion Mobility Coefficients Using Voltage Sweep Multiplexing. *J. Am. Soc. Mass Spectrom.* **2019**, *30* (6), 977−986.
(28) Keelor, J. D.; Zambrzycki, S.; Li, A.; Clowers, B. H.; Fernández, F. M. Atmospheric Pressure Drift Tube Ion Mobility−Orbitrap Mass Spectrometry: Initial Performance Characterization. *Anal. Chem.* **2017**, *89* (21), 11301−11309.
(29) Poltash, M. L.; McCabe, J. W.; Shirzadeh, M.; Laganowsky, A.; Russell, D. H. Native IM-Orbitrap MS: Resolving What Was Hidden. *TrAC Trends Anal. Chem.* **2020**, *124*, 115533.
(30) Kwantwi-Barima, P.; Reinecke, T.; Clowers, B. H. Increased Ion Throughput Using Tristate Ion-Gate Multiplexing. *Analyst* **2019**, *144* (22), 6660−6670.
(31) Davis, A. L.; Liu, W.; Siems, W. F.; Clowers, B. H. Correlation Ion Mobility Spectrometry. *Analyst* **2017**, *142* (2), 292−301.
(32) Reinecke, T.; Naylor, C. N.; Clowers, B. H. Ion Multiplexing: Maximizing Throughput and Signal to Noise Ratio for Ion Mobility Spectrometry. *TrAC Trends Anal. Chem.* **2019**, *116*, 340−345.
(33) Kwantwi-Barima, P.; Reinecke, T.; Clowers, B. H. Enabling Resolution of Isomeric Peptides Using Tri-State Ion Gating and Fourier-Transform Ion Mobility Spectrometry. *Int. J. Ion Mobil. Spectrom.* **2020**, *23* (2), 133−142.
(34) Kirk, A. T.; Grube, D.; Kobelt, T.; Wendt, C.; Zimmermann, S. High-Resolution High Kinetic Energy Ion Mobility Spectrometer Based on a Low-Discrimination Tristate Ion Shutter. *Anal. Chem.* **2018**, *90* (9), 5603−5611.
(35) Bradbury, N. E.; Nielsen, R. A. Absolute Values of the Electron Mobility in Hydrogen. *Phys. Rev.* **1936**, *49* (5), 388−393.
(36) Tyndall, A. M.; Powell, C. F. The Mobility of Ions in Pure Gases. *Proc. R. Soc. Lond. A* **1930**, *129*, 162.
(37) Chen, C.; Tabrizchi, M.; Li, H. Ion Gating in Ion Mobility Spectrometry: Principles and Advances. *TrAC Trends Anal. Chem.* **2020**, *133*, No. 116100.
(38) Bohnhorst, A.; Kirk, A. T.; Zimmermann, S. Toward Compact High-Performance Ion Mobility Spectrometers: Ion Gating in Ion Mobility Spectrometry. *Anal. Chem.* **2021**, *93* (15), 6062−6070.
(39) Lee, S.; Ewing, M. A.; Nachtigall, F. M.; Kurulugama, R. T.; Valentine, S. J.; Clemmer, D. E. Determination of Cross Sections by Overtone Mobility Spectrometry: Evidence for Loss of Unstable Structures at Higher Overtones. *J. Phys. Chem. B* **2010**, *114* (38), 12406−12415.
(40) Zucker, S. M.; Ewing, M. A.; Clemmer, D. E. Gridless Overtone Mobility Spectrometry. *Anal. Chem.* **2013**, *85* (21), 10174−10179.
(41) Chen, H.; Chen, C.; Huang, W.; Li, M.; Xiao, Y.; Jiang, D.; Li, H. Miniaturized Ion Mobility Spectrometer with a Dual-Compression Tristate Ion Shutter for On-Site Rapid Screening of Fentanyl Drug Mixtures. *Anal. Chem.* **2019**, *91* (14), 9138−9146.
(42) Thoben, C.; Raddatz, C.-R.; Lippmann, M.; Salehimoghaddam, Z.; Zimmermann, S. Electrospray Ionization Ion Mobility Spectrometer with New Tristate Ion Gating for Improved Sensitivity for Compounds with Lower Ion Mobility. *Talanta* **2021**, *233*, No. 122579.
(43) Reinecke, T.; Clowers, B. H. Implementation of a Flexible, Open-Source Platform for Ion Mobility Spectrometry. *HardwareX* **2018**, *4*, No. e00030.
(44) Garcia, L.; Saba, C.; Manocchio, G.; Anderson, G. A.; Davis, E.; Clowers, B. H. An Open Source Ion Gate Pulser for Ion Mobility Spectrometry. *Int. J. Ion Mobil. Spectrom.* **2017**, *20* (3), 87−93.
(45) Cabrera, E. R.; Clowers, B. H. Synchronized Stepped Frequency Modulation for Multiplexed Ion Mobility Measurements. *J. Am. Soc. Mass Spectrom.* **2022**, *33* (3), 557−564.
(46) Cabrera, E. R.; Clowers, B. H. Considerations for Generating Frequency Modulation Waveforms for Fourier Transform-Ion Mobility Experiments. *J. Am. Soc. Mass Spectrom.* **2022**, *33* (10), 1858−1864.
(47) Levin, M.; Krisilov, A.; Zon, B.; Eiceman, G. The Effect of Space Charge in Ion Mobility Spectrometry. *Int. J. Ion Mobil. Spectrom.* **2014**, *17* (2), 73−77.
(48) May, J. C.; Jurneczko, E.; Stow, S. M.; Kratochvil, I.; Kalkhof, S.; McLean, J. A. Conformational Landscapes of Ubiquitin, Cytochrome c, and Myoglobin: Uniform Field Ion Mobility Measurements in Helium and Nitrogen Drift Gas. *Int. J. Mass Spectrom.* **2018**, *427*, 79−90.
(49) Allen, S. J.; Eaton, R. M.; Bush, M. F. Structural Dynamics of Native-Like Ions in the Gas Phase: Results from Tandem Ion Mobility of Cytochrome c. *Anal. Chem.* **2017**, *89* (14), 7527−7534.
(50) Dickinson, E. R.; Jurneczko, E.; Pacholarz, K. J.; Clarke, D. J.; Reeves, M.; Ball, K. L.; Hupp, T.; Campopiano, D.; Nikolova, P. V.; Barran, P. E. Insights into the Conformations of Three Structurally Diverse Proteins: Cytochrome c, P53, and MDM2, Provided by Variable-Temperature Ion Mobility Mass Spectrometry. *Anal. Chem.* **2015**, *87* (6), 3231−3238.

https://doi.org/10.1021/jasms.2c00274
J. Am. Soc. Mass Spectrom. 2023, 34, 101−108